Applied Radiation and Isotopes 118 (2016) 140–148

Contents lists available at ScienceDirect

Applied Radiation and Isotopes

journal homepage: www.elsevier.com/locate/apradiso

Monte Carlo study of neutron-ambient dose equivalent to patient in treatment room

A. Mohammadi[a], H. Afarideh[a], F. Abbasi Davani[b], M. Ghergherehchi[c,*], A. Arbabi[d]

[a] Energy Engineering and Physics Department, Amir Kabir University of Technology, Tehran, Iran
[b] Radiation Application Group, Shahid Beheshti University, Tehran, Iran
[c] College of Information & Communication Engineering, School of Electronics and Electrical Engineering, Sungkyunkwan University, Suwon, Republic of Korea
[d] Department of Medical Physics, Imam Hosein Hospital, Shahid Beheshti Medical University, Tehran, Iran

ARTICLE INFO

Keywords:
Scattering factor
Thermal factor
Medical linear accelerator
Treatment room

ABSTRACT

This paper presents an analytical method for the calculation of the neutron ambient dose equivalent H* (10) regarding patients, whereby the different concrete types that are used in the surrounding walls of the treatment room are considered. This work has been performed according to a detailed simulation of the Varian 2300C/D linear accelerator head that is operated at 18 MV, and silver activation counter as a neutron detector, for which the Monte Carlo MCNPX 2.6 code is used, with and without the treatment room walls. The results show that, when compared to the neutrons that leak from the LINAC, both the scattered and thermal neutrons are the major factors that comprise the out-of field neutron dose. The scattering factors for the limonite-steel, magnetite-steel, and ordinary concretes have been calculated as 0.91 ± 0.09, 1.08 ± 0.10, and 0.371 ± 0.01, respectively, while the corresponding thermal factors are 34.22 ± 3.84, 23.44 ± 1.62, and 52.28 ± 1.99, respectively (both the scattering and thermal factors are for the isocenter region); moreover, the treatment room is composed of magnetite-steel and limonite-steel concretes, so the neutron doses to the patient are 1.79 times and 1.62 times greater than that from an ordinary concrete composition. The results also confirm that the scattering and thermal factors do not depend on the details of the chosen linear accelerator head model. It is anticipated that the results of the present work will be of great interest to the manufacturers of medical linear accelerators.

1. Introduction

Medical linear accelerators of different models and electron energies (4–25 MeV) are widely used for radiotherapy. For radiation protection purposes, these devices are normally installed in treatment rooms that are composed of particular dimensions and are constructed with the use of different concrete types. The unwanted neutrons are produced through the electronuclear (e,én), single photonuclear (γ,n), and double photonuclear (γ,2n) reactions of the high-energy electrons and photons that bombard the high-Z material targets when the energy of the photon beam is greater than approximately 7 MeV (Hsu et al., 2010; Mesbahi et al., 2010; Naseri and Mesbahi, 2010; Thalhofer et al., 2014). The produced neutrons basically lose their initial energies through the multiple scatterings that are from the different elements of the treatment room walls, and they are then scattered back to the treatment room where they may reach the patient. The scattered photons and neutrons from the treatment room are the main dosage sources in the out-of field region (Biltekin et al., 2015; Followill et al., 2003; Liu et al., 2011; Takam, 2010; Vega-Carrillo et al., 2007; Xu et al., 2008). The measurement and applied correction factor of the scattered radiation contribution are recommended by the IAEA for all of the reference radiations at certain distances. The basic sources of scattered radiations are the walls, floor, and ceiling, as well as the other objects that normally exist in the treatment room, and the use of the shadow cone is one of the recommended methods for the measurement of the scattered neutrons in the irradiation room (IAEA, 2000a, 200b; ISO8529, 1998). The quality of radiation therapy is highly dependent on the photon doses that are delivered to the patient. In general, the delivered dose is due to the direct and scattered radiations in the treatment room (Bartesaghi, 2007); for example, the emphasis of both the Safety Series Report No.16 (2000) and the ISO8529–3 (2000) is a maximal elimination of the scattered neutrons for the neutron dosimeters and the field calibration, and this is also confirmed for the calibration of the gamma dosimeters. With regard to radiotherapy patients, the ICRP publication 103 (ICRP, 2007) calls for *"... delivery of the required dose to the volume to be treated, avoiding unnecessary*

* Corresponding author.
E-mail addresses: hafarideh@aut.ac.ir (H. Afarideh), mitragh@skku.edu (M. Ghergherehchi).

http://dx.doi.org/10.1016/j.apradiso.2016.07.009
Received 12 April 2016; Received in revised form 5 July 2016; Accepted 11 July 2016
Available online 12 July 2016
0969-8043/ © 2016 Published by Elsevier Ltd.

exposure of healthy tissues."

As described by Pena et al., 2005 the three energy ranges of the neutrons in the treatment room are as follows: Fast neutrons (0.1 MeV to 10 MeV), epithermal neutrons (0.50 MeV to 0.1 MeV), and thermal neutrons (less than 0.50 eV). The three ranges are produced via the interactions between the high energy photons with the LINAC head components and the treatment room walls (Pena et al., 2005). In medical linear accelerators, bremsstrahlung X-rays are produced through the interaction of the high-energy electrons with the target. The scattering and thermal neutron cross sections, the different (γ,n) threshold energies of the materials in the walls, and the linear accelerator installations along the photon path are the most important factors for the determination of the scattering and thermal factors. The unwanted doses of the extra neutrons and photons are not prescribed, as they are of course non-therapeutic; also, the energy spectrum of the produced neutrons ranges from thermal to several MeVs, based on the initial energy of the electron beam (up to 25 MeV). In the treatment room, the average energy of the produced neutrons varies from 0.1 MeV to 2 MeV, and the radiation weighting factor of 20 is recommended for these deeply penetrating particles with a high radiobiological effectiveness (RBE) (NCRP Report 116., 1993); for this reason, their contributions to a patient's out-of field dose that is relative to the direct dose from the photon beam can be important with respect to the risk of cancer inducement (Naseri and Mesbahi, 2010).

Measurements of the photo neutron contaminated components (direct, scattered, and thermal neutron fluences and spectra) are possible when either a passive or active neutron detection system is used in the treatment room. For the passive detectors, the energy spectrum and the ambient dose equivalent of the neutrons that are produced by a 15 MV Varian iX medical LINAC have been measured with a Bonner sphere spectrometer in the out-of field region, and as the thermal-neutron detector, the TLD pair (TLD600 and TLD700) was placed at the center of each sphere (Benites-Rengifo et al., 2014). Recently, a pairs of dosimeters that comprise the TLD 600 (^{6}LiF: Mg, Ti) and the TLD 700 (^{7}LiF: Mg, Ti) were placed inside a paraffin sphere with a 20 cm diameter, and they were used to measure the ambient dose equivalent [$H^{*}(10)$] of the neutrons at different positions around the LINAC head (Ramírez et al., 2016). In another work, the CR-39 solid-state nuclear track detectors (SSNTDs) were used to investigate the variations of the fast neutron intensity at the different positions of the treatment room (Shweikani and Anjak, 2015). The neutron fluence $\phi(l)$ at the point-of-interest that is located at the distance l from the center of the LINAC head, and that is measured according to the unit n cm^{-2}/Gy X-ray, is determined through the use of neutron detector reference instruments (IAEA, 2000a, 2000b). For the active detectors, however, there are no available data in the literature.

A certain fraction of the neutron dose that is delivered to the patient is due to the scattering that is off the walls of the treatment room. The production and backscattering of the photoneutrons from a simple wall with a thickness of 2.5 m and dimensions of 6×6 m^2, in width and length, respectively, for example, have been calculated; for this purpose, the photon and neutron beam spectra that were used as the photon and neutron sources, respectively, originated from the 18 MV-beam target of the Varian LINAC (Mesbahi et al., 2010). Notably, the neutron fluence has only been calculated at the inner maze entrance with the use of 10 cm and 20 cm radius scoring cells for the field size with dimensions of 30×30 cm^2 (Mesbahi et al., 2012). In addition, the room-return neutrons at the spherical cavity with different radii from 150 cm to 1010 cm, and with the use of ordinary concrete (2.35 g/cm^3), have been calculated with and without air; for this purpose, the monoenergetic neutron source has been considered. The energy spectra of neutrons have also been reported for different cavities (Vega-Carrillo et al., 2007).

In this study, the scattering and thermal neutron factors of the bunker have been calculated in terms of the installation of the Varian 2300 C/D medical LINAC; therefore, the scattering and thermal neutron factors of the bunker have been calculated for a case where the concrete type regarding the walls is important for the design of the bunker. For the purpose of this study, the actual detector (silver activation counter) has been simulated to calculate the neutron fluences and doses, and the configuration of the LINAC head, the treatment room with different concrete types, and the actual activation counter have been simulated with the use of the Monte Carlo MCNPX 2.6 code. The activation counter is commonly used for the measurement of the neutron yield of the pulsed neutron sources such as the plasma focus and the Tokamak (Ragabi moghaddam and Abbasi Davani, 2009). The selected medical linear accelerator has not been used as a multi-leaf collimator (MLC). It should be noted that the calculated contributions (Mao et al., 1997) of each of the different parts of the LINAC head such as the target, flattening filter, and primary and secondary collimators are different to the total neutron source strength/fluence at any point in the treatment room. Also, for the 18 MV-photon case, the neutron contamination has been calculated at the isocenter with and without a flattening filter (Mesbahi et al., 2010). According to this study, the calculations of the scattering and thermal factors are based on the neutron fluences for $E_n > 0.5$ eV and $E_n < 0.5$ eV, respectively. The influence of the MLC and the other components on the scattering and thermal factors and the neutron doses can be calculated later to obtain the total of the neutron fluences.

The main purposes of the present work are as follows:

1. The transportation of the coupled electron-photon-neutron modes
2. The selection of a measurable arrangement of the silver activation counter to ensure its capability as a reliable neutron detector for neutron fluence calculations, whereby the Varian 2300C/D linear accelerator head is used as an intense pulsed neutron source, and a treatment room with usable dimensions and different types of concretes has been employed.
3. A determination of the scattering and thermal factors of treatment rooms where, along the patient couch, the concrete construction is either limonite-steel, magnetite-steel, or ordinary concretes that includes the use of the Monte Carlo method for different photon fields and positions.
4. The calculation of the received backscattered neutron dose contributions from the walls of the treatment room (out-field) to the patient at the isocenter.

2. Materials and methods

2.1. Linear accelerator head simulation

The full details of the 2300C/D Varian medical linear accelerator head that is operated at 18 MV have been simulated using the Monte Carlo MCNPX 2.6 code. The model includes a LINAC that is operated at the dual-photon energies of 6 MeV and 18 MeV, and the multiple electron energies of 6 MeV, 9 MeV, 12 MeV, 16 MeV, 18 MeV, and 20 MeV; but, an MLC is not included here. The diameter of the pencil-electron beam is 1 mm (Podgorsak, 2005). The electron-photon-neutron modes and all of the main components of the medical LINAC head were considered for the simulation. The main parts of the LINAC head consist of a target (W), copper as the cooling section that is in front of the target, a Be window, a primary collimator (W), a flattening filter (Fe+Ta), and upper and lower jaws (W), all of which have been simulated to investigate the neutron production. Both the LINAC head and the typical treatment room that were used in the simulations are shown in Figs. 1 and 2, whereby the former shows the details of the LINAC head, while Fig. 2 illustrates the treatment room dimensions, the position of the activation counter, and the direction of the LINAC head. The number of the primary particle histories (i.e., electrons) has been set to 2.00×10^9.

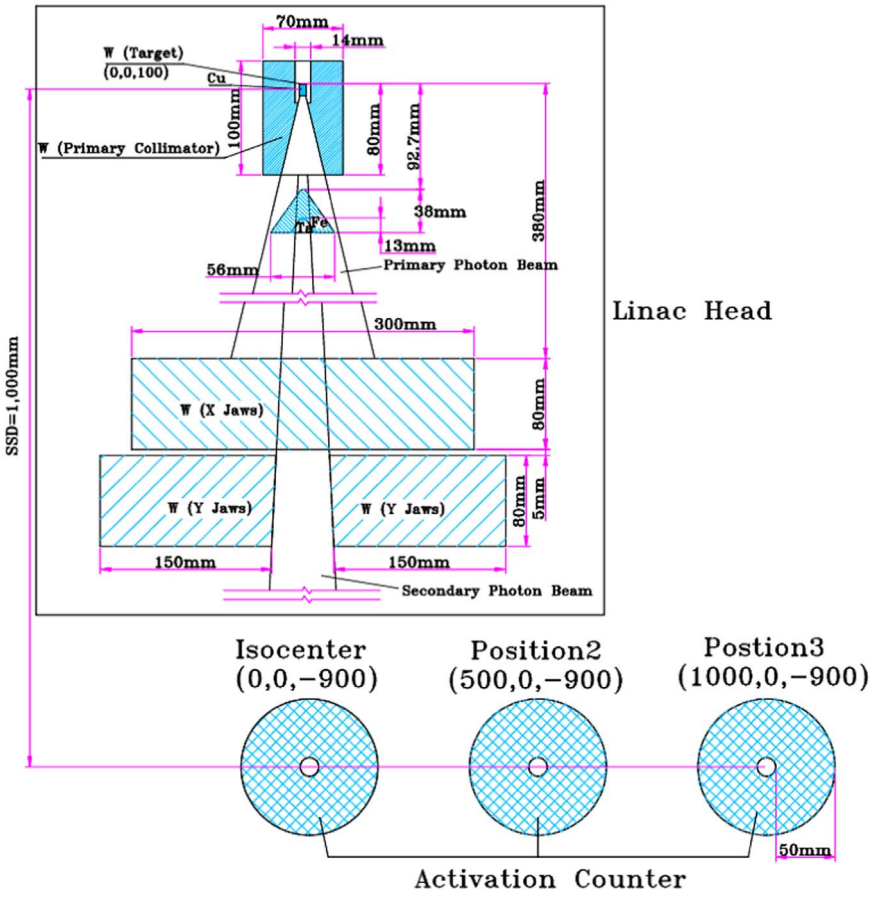

Fig. 1. LINAC head and activation counter at three different positions (position 1 or isocenter, position 2 and position 3); dimensions in mm.

2.2. Silver activation counter simulation

The activation counter is made of a cylindrical natural-silver foil (^{107}Ag and ^{109}Ag isotopes), and is of a 160 mm length and a 10.5 g/cm^3 density. The inner and outer diameters are 16 mm and 16.025 mm, respectively. To calculate the fast neutron fluencies (n cm^{-2}/GyX-ray) that originate from both of the LINAC head and the treatment room, the thicknesses of the polyethylene neutron moderators (of a 0.935 g/cm^3 density) have been optimized for the in-field and out-of field detections. For the registration of the fast neutron fluences, the silver foil is placed inside the neutron moderator while the thermal neutron fluence is calculated through the removal of the neutron moderator. The neutron fluence spectra that correspond to the in-field and out-of field of the photon beam are different; that is, the in-field neutron fluences are the neutrons that originate from either the target and the flattening filter of the LINAC head and have travelled through the photon field, while the out-of field neutrons are those that have been scattered off the treatment room walls.

The thermal neutron cross sections of ^{107}Ag and ^{109}Ag isotopes are 40 *b* and 113 *b*, respectively. The thermal neutron capture by the ^{107}Ag and ^{109}Ag isotopes occur after well-known reactions, as follows (Gentilini et al., 1980):

$$n_{th}{}^{109} + Ag \rightarrow \gamma + {}^{110}Ag \rightarrow {}^{110}Cd + \beta^{-}(E_{\beta} = 2.82\ \text{MeV and}\ T_{1/2} = 24.2\ \text{s}) \quad (1)$$

$$n_{th} + {}^{107}Ag \rightarrow \gamma + {}^{108m}Ag \rightarrow {}^{108}Cd + \beta^{-}(E_{\beta} = 1.49\ \text{MeV and}\ T_{1/2} = 144.6\ \text{s}) \quad (2)$$

For a typical irradiation time duration, the silver activity *A(t)* may be obtained as follows:

$$A(t) = N\sigma\Phi(1 - e^{-\lambda t}), \quad (3)$$

where N is the number of Ag nuclei per cm^3, σ is the microscopic thermal neutron cross section, Φ is the total neutron fluence (n cm^{-2}) at the detector position, λ is the decay constant, and t is the irradiation time. It is also assumed that the induced activity of the silver foil is proportional to the initial neutron beam fluence. For both the ^{107}Ag and ^{109}Ag isotopes, Eq. (3) may be rewritten as follows:

$$A = \Phi[N_{107}\sigma_{107}(1 - exp(-\lambda_{108}t) + N_{109}\sigma_{109}(1 - exp(-\lambda_{110}t))] \quad (4)$$

For a relatively long irradiation time for example, 1000 s (compared with the half-lives of 24.2 s and 144.6 s), the term (1-e$^{-\lambda t}$) has been fairly set to 1; therefore, the following equation applies:

$$A_{sat} = \Phi(N_{107}\,\sigma_{107} + N_{109}\sigma_{109}) \quad (5)$$

The total reaction rate in the silver foil can be simply calculated using Tally F4 (i.e., the volumetric flux or the average track lengths per volume for the particle-of-interest) together with a reaction number of 102; alternatively, 487 keV gamma rays, which are emitted following the neutron-induced beta decay in the silver, can be registered. The induced activities (Bq/GyX-ray) that are due to the fast and thermal photoneutrons have been calculated at the isocenter (position 1), at 0.5 m (position 2), and at 1 m (position 3), far from the central-beam axis, for different photon field sizes. The spatial coordinates of isocenter (position 1) to position 3 are (0,0,−0.9), (0.5,0,−0.9), and (1,0,−0.9), respectively, where the origin (i.e., (0,0,0)) is the center of the treatment room floor. The spatial coordinates of the LINAC head is (0, 0,0.1)(see Fig. 2).

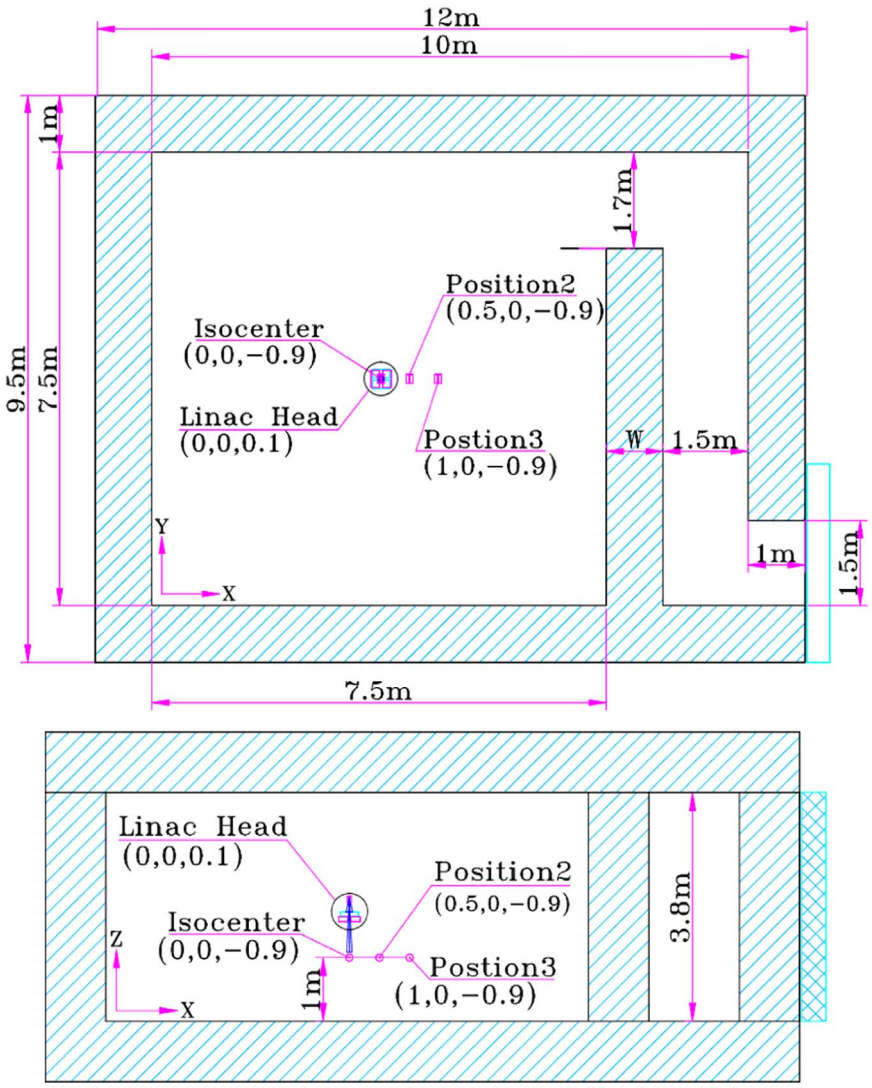

Fig. 2. Treatment room, orientation and location of the LINAC head, and activation counter (dimensions in m).

2.3. Treatment room simulation

To determine the scattering and thermal factors, all of the calculations have been undertaken along the patient couch, with and without the treatment room walls, at the three above-specified positions. The photon field sizes have been changed from 0×0 cm^2 to 40×40 cm^2 in 5×5 cm^2 step sizes. The considered treatment room dimensions are 7.5×7.5×3.8 m^3, where the 1 m thick walls are made of three different concretes with different densities that are specified in parentheses, as follows: ordinary (2.35 g/cm^3), limonite-steel (4.54 g/cm^3), and magnetite-steel (4.64 g/cm^3). The weight fraction of these concretes are listed in Table 1 (McConn et al., 2011), and the threshold energies of the (γ.n) reaction of the elements for the selected types of concretes, the silver activation counter, and the LINAC head components are listed in Table 2. For a special point-of-interest in the treatment room (e.g., along the patient couch), the total fluences of the neutrons (n cm^{-2}/GyX-ray) can be calculated as follows (IAEA, 2006):

$$\Phi_{total} = \varphi_{direct} + \varphi_{scatter} + \varphi_{thermal}, \quad (6)$$

where φ_{direct} is the neutron fluence (n cm^{-2}/GyX-ray) with an energy greater than 0.5 eV and that exclusively originates from the LINAC head; $\varphi_{scatter}$ represents the neutron fluence (n cm^{-2}/GyX-ray) with an energy greater than 0.5 eV that is from all of the components, except the LINAC head, that are inside the treatment room; and $\varphi_{thermal}$ is the thermal neutron fluence (n cm^{-2}/GyX-ray) with an energy less than 0.5 eV and that is from the inside of the LINAC head, the patient coach, the indoor air, the treatment room walls, and any other facility that is inside the treatment room. To calculate the neutron fluence and dose, and for the sake of simplicity, the neutrons with the energies $E_n < 0.5$ eV and $E_n > 0.5$ eV have therefore been considered as thermal and fast neutrons, respectively. Due to the difference between the fast and thermal neutron fluences/doses that were produced from the interactions with the different concretes, it seems that the floor materials are

Table 1
Weight fractions of three concrete types (McConn Jr. et al., 2011).

Weight fraction					
Ordinary concrete		Limonite and steel		Magnetite and steel	
H	0.008485	H	0.006840	H	0.002374
C	0.050064	O	0.156222	O	0.137678
O	0.473483	Mg	0.001545	Mg	0.003669
Mg	0.024183	Al	0.006399	Al	0.010358
Al	0.036063	Si	0.014784	Si	0.015753
Si	0.145100	K	0.000883	Ca	0.055675
S	0.002970	Ca	0.057590	Ti	0.015969
K	0.001697	V	0.000883	V	0.000647
Ca	0.246924	Fe	0.754854	Fe	0.757877
Fe	0.011031				

Table 2
The (γ,n) reaction threshold energies of the elements for the selected types of concretes, LINAC head components, and silver activation counter (IAEA, 2000a).

Element		Abundance	(γ,n) reaction threshold energy (MeV)
Be		100.00	1.67
C		98.89	18.72
O		99.76	15.66
Mg	^{24}Mg	78.99	16.53
	^{25}Mg	10.00	7.23
	^{26}Mg	11.01	11.90
Al		100.00	13.60
Si	^{28}Si	92.23	17.18
	^{29}Si	4.67	8.47
	^{30}Si	3.10	10.61
S	^{32}S	95.02	15.04
	^{33}S	0.75	8.64
	^{34}S	4.21	11.42
K	^{39}K	93.26	13.08
	^{40}K	6.73	10.10
Ca	^{40}Ca	96.94	15.64
	^{42}Ca	0.65	11.48
	^{43}Ca	0.14	7.93
	^{44}Ca	2.09	11.13
V		99.75	11.05
Fe	^{54}Fe	5.90	13.38
	^{56}Fe	91.72	11.20
	^{57}Fe	2.10	7.65
	^{58}Fe	0.28	10.04
Cu	^{63}Cu	69.17	10.85
	^{65}Cu	30.83	9.91
Ag	^{107}Ag	51.84	9.54
	^{109}Ag	48.16	9.19
Ta		99.99	7.58
W	^{180}W	0.12	8.41
	^{182}W	26.30	8.07
	^{183}W	14.28	6.19
	^{184}W	30.70	7.41
	^{186}W	28.60	7.19

necessarily considered in any simulation that is regarding neutron fluences/doses.

Each term of Eq. (6) is rewritten in Eq. (7) (IAEA, 2006), as follows:

$$\varphi_{total}=\frac{Q}{4\pi d^2}+\frac{5.4Q}{S}+\frac{1.26Q}{S}, \quad (7)$$

where Q is the neutron source strength value (n/GyX-ray) of the LINAC head, d is the distance (m) for the point-of-interest that is a far distance from the target, and S is the total area of the treatment room (m^2) (IAEA, 2006). The direct neutrons (fast and thermal) are the neutrons that are delivered to the silver activation counter at all of the positions when the treatment room walls are removed, while the scattered neutrons are delivered when the walls are present. The scattering factor (SF) is defined as the difference between the produced fast neutron fluence at each position, with and without the walls, as follows:

$$SF=\frac{FNF_C - FNF_{NC}}{FNF_{NC}}, \quad (8)$$

where FNF_C and FNF_{NC} are the produced fast neutron fluences ($E_n > 0.5\ eV$) with and without the treatment room walls, respectively.

The thermal factor (TF) is defined as the difference between the produced thermal neutron fluence at each position with and without the walls, as follows:

$$TF=\frac{TNF_C - TNF_{NC}}{TNF_{NC}}, \quad (9)$$

where TNF_C and TNF_{NC} are the thermal neutron fluences ($E_n < 0.5\ eV$) with and without the treatment room walls, respectively. It is assumed here that the total electron beam current of the medical LINAC that is on the target is 76 μA, and that it is approximately equal to 4.74×10^{14} e, which is equivalent to 1 Gy X-ray dose at isocenter

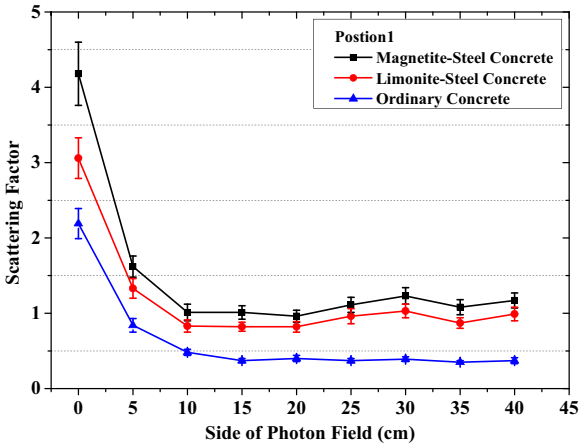

Fig. 3. Scattering factors of the treatment room at position 1 for limonite-steel, magnetite-steel, and ordinary concretes.

(Mohammadi et al., 2016). The results have been obtained through a multiplication of this conversion factor for all of the calculated values.

To calculate the neutron ambient dose equivalent, the average neutron energy spectrum over the total surface of the silver activation counter must be determined first, in addition to the use of the appropriate conversion coefficients that are normally used in the radiation protection data sheets (ICRP, 1996).

3. Results and discussion

3.1. Scattering factors

Fig. 3 shows a comparison of the scattering factors at isocenter (position 1) for the different concrete types and photon field sizes. According to Fig. 3, the scattering factors are 1.081 ± 0.098, 0.903 ± 0.087, and 0.387 ± 0.045 for the magnetite-steel, limonite-steel, and ordinary concretes, respectively, for field sizes that are larger than the range from 10×10 cm^2 to 40×40 cm^2; that is, the scattering factors do not exhibit significant changes for field sizes ranging from 10×10 cm^2 to 40×40 cm^2. The scattered neutron fluence is greater than that of the direct neutrons in the treatment room for the closed field and represents a small contribution for the 5×5 cm^2 field size, and this is why the scattering factors are greater than the other fields. The results here confirm that the neutron fluencies are strongly dependent on the photon field sizes at the isocenter, and this is in agreement with other works (Al-Ghamdi et al., 2008; Lin et al., 2001); however, the fast neutron fluence is increased as the photon field size increases.

Fig. 4 shows a comparison between the scattering factors along the patient couch at position 2 for all of the field sizes. According to Fig. 4, the scattering factors decrease as the field size increases up to 10×10 cm^2, but then increases for larger field sizes. The scattering factors of the limonite-steel, magnetite-steel, and ordinary concretes represent variation ranges of 1.10–3.41, 1.73–4.50, and 0.77–2.55, respectively, for the photon field sizes from 10×10 cm^2 to 40×40 cm^2; moreover, for the regions near the edge of the photon field, the contribution of the scattered neutrons is more than those of the farther regions. These results provide the reason for why the scattering factors increase according to the increasing of the photon field size.

Fig. 5 illustrates the scattering factors of the three types of concrete that are along the patient couch at position 3. According to Fig. 5, the scattering factors of the limonite-steel, magnetite-steel, and ordinary concretes vary from 2.24 to 2.8, 2.96 to 3.6, and 1.46 to 1.6, respectively, for the different photon-field sizes. By comparing Fig. 5 with Fig. 4, the variation ranges of the scattering factors at position 3 are less than those of the scattering factors at position 2 1.10–3.41, 1.73–4.50, and 0.77–2.55 for the limonite-steel, magnetite-steel, and

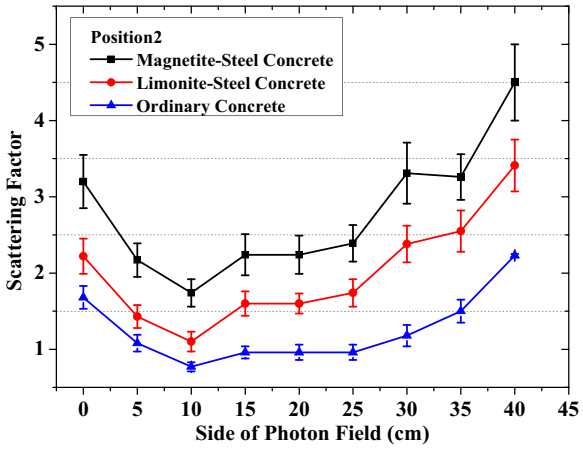

Fig. 4. Scattering factors of the treatment room at position 2 for limonite-steel, magnetite-steel, and ordinary concretes.

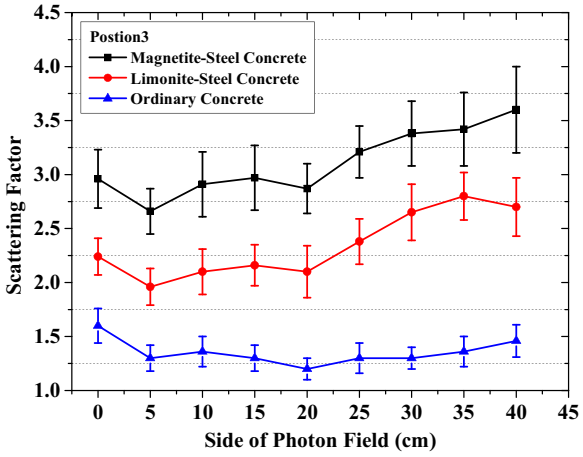

Fig. 5. Scattering factors of the treatment room at position 3 for limonite-steel, magnetite-steel, and ordinary concretes.

ordinary concretes, respectively); therefore, the scattering factors do not significantly change at position 3. According to Figs. 3–5, the scattering factors are greater than the unity for all of the concretes used in this work, with the exception of the ordinary concrete, at the isocenter; therefore, the large neutron-fluence fractions that are delivered to the patient are due to the scattering neutrons. Since the average energy of the scattering neutrons (the out-of field neutrons) is less than that of the neutrons that originate from the target and the flattening filter (the direct neutrons or in-field neutrons), the conversion coefficient of the scattering neutrons is less than that of the direct neutrons; therefore, the contribution of the scattering neutron dose that is delivered to the patient is less than that of the scattering neutron fluence.

The scattering neutron fluence basically depends on the neutron source strength and spectrum of the LINAC head, the treatment room dimensions, and the wall concrete type. The scattering neutron equivalent doses are strongly dependent on both the average energies and the average fluences of the scattering neutrons. Through a comparison of Figs. 3–5, the scattering factors increase in accordance with the distance from the isocenter. The larger fractions of the doses that are received by the patient may be related to the scattering neutrons at the photon out-of field.

Fig. 6 shows the neutron elastic scattering cross sections of iron, oxygen, and calcium nuclei for a range of neutron energies, wherein the iron represents the largest cross section. Due to the high weight fraction of the iron in the magnetite-steel and limonite-steel concretes, the scattering factors become greater than that of ordinary concrete for all of the field sizes.

3.2. Thermal factors

Fig. 7 shows the thermal factors of the treatment room at isocentrt (position 1) for the limonite-steel, magnetite-steel, and ordinary concretes. According to Fig. 7, the thermal factors decrease in accordance with an increasing of the photon field size at the isocenter up to 15×15 cm^2, and they then become flat with further increases of the field size. The thermal factors of the limonite-steel and magnetite-steel concretes are approximately the same, while the thermal factor of the ordinary concrete is greater than those of the limonite-steel and magnetite-steel concretes. Also, the thermal neutron fluence from the LINAC head is less than that from the treatment room; therefore, the thermal factors are significantly greater than the scattering factors.

Fig. 8 illustrates the thermal factors of the treatment room at position 2 for the limonite-steel, magnetite-steel, and ordinary concretes. According to Fig. 8, the thermal factors of the magnetite-steel, limonite-steel, and ordinary concretes are the same for the field sizes from 5×5 cm^2 to 25×25 cm^2, and they then increase in accordance with an increasing of the field size.

Fig. 9 shows a comparison of the thermal factors at position 3 for the magnetite-steel, limonite-steel, and ordinary concretes. According to the data of Fig. 9 and the standard deviations, the thermal factors remain approximately constant for all of the photon field sizes at position 3.

3.3. Relationship between total neutron fluences, scattering, and thermal factors

In this section, a study of the relationship between the total neutron fluences, the scattering, and the thermal factors of the treatment room that is for the attainment of a general formula is presented. The total neutron fluences at the isocenter without the treatment room walls is equals to the summation of the direct fast and thermal neutron fluencies that originate from the LINAC head. As discussed earlier, the fast neutron fluencies correspond to the neutrons with energies that are more than the cadmium cut-off (i.e., $E_n > 0.5$ eV), while the thermal neutrons are those with $E_n < 0.5$ eV. For a given field size at the isocenter, the total neutron fluence without the treatment room (ϕ_{direct}) has been obtained as follows:

$$\varphi_{direct}=\frac{Q}{4\pi d^2}=\varphi_{fast}+\varphi_{thermal}, \quad (10)$$

where Q is the neutron source strength value of the LINAC head, and d the distance(m) of the interest point (e.g., the isocenter) from the target of the LINAC head. The scattering neutron fluence ($\phi_{scatter}$) that

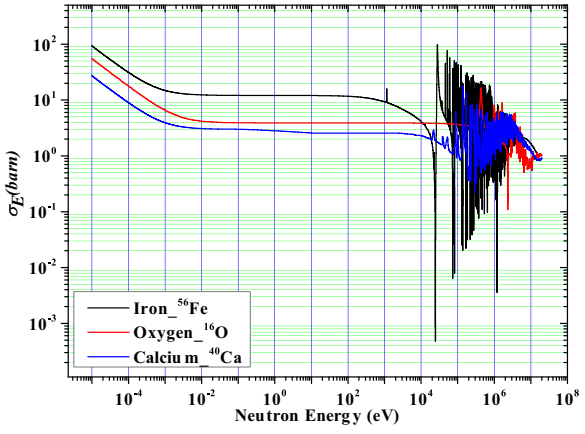

Fig. 6. Neutron elastic scattering cross sections of the iron, oxygen, and calcium nuclei (JANIS).

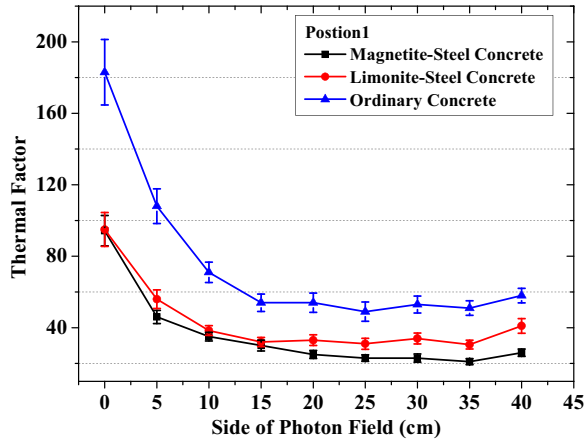

Fig. 7. Thermal factors of the treatment room at position 1 for limonite-steel, magnetite-steel, and ordinary concretes.

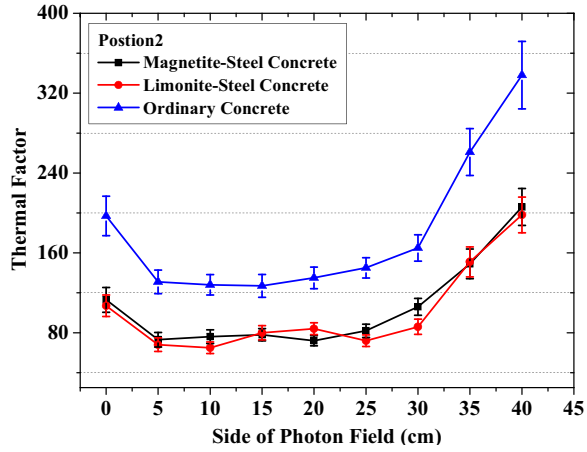

Fig. 8. Thermal factors of the treatment room at position 2 for limonite-steel, magnetite-steel, and ordinary concretes.

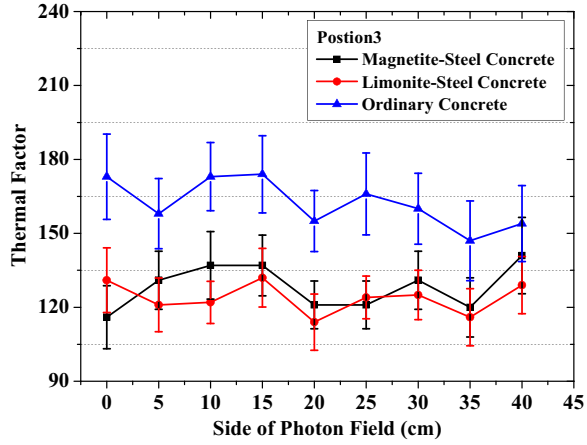

Fig. 9. Thermal factors of the treatment room at position 3 for limonite-steel, magnetite-steel, and ordinary concretes.

originates from just the treatment room has been calculated as follows:

$$\varphi_{scatter} = a\varphi_{fast} + b\varphi_{thermal}, \quad (11)$$

where a and b are the scattering and thermal factors, respectively. The total neutron fluence at the isocenter in the treatment room, however, is equal to the following:

$$\Phi_{total} = \varphi_{direct} + \varphi_{scatter}, \quad (12)$$

Table 3
Total neutron fluence (n cm^{-2}/GyX-ray) at the isocenter for ordinary, magnetite-steel, and limonite-steel concretes.

Field size (cm^2)	Total neutron fluence (n cm^{-2}/GyX-ray)_Isocenter					
	Total neutron fluence (n cm^{-2}/GyX-ray) _Ordinary Concrete		Total neutron fluence (n cm^{-2}/GyX-ray) _Magnetite-steel		Total neutron fluence (n cm^{-2}/GyX-ray) _Limonite-steel	
	$(SF + 1)\phi_{fast}$	$(TF + 1)$ ϕthermal	$(SF + 1)$ ϕ_{fast}	$(TF + 1)$ ϕthermal	$(SF + 1)$ ϕ_{fast}	$(TF + 1)$ ϕthermal
Closed	3.190	184	5.17	95.26	4.06	96.53
5×5	1.845	109	2.61	46.20	2.33	56.50
10×10	1.475	73	2.00	35.94	1.84	39.64
15×15	1.373	55	2.01	25.68	1.82	33.33
20×20	1.390	55.69	1.96	23.50	1.82	34.18
25×25	1.373	50.21	2.11	23.85	1.96	31.88
30×30	1.373	53.50	2.24	23.14	2.03	34.50
35×35	1.357	52.00	2.09	21.31	1.87	31.51
40×40	1.373	53.29	2.17	27.16	2.00	41.47
Average	15×15 cm^2 to 40×40 cm^2 Φ_{total} = (1.371 ± 0.01)φ_{fast} + (53.28 ± 1.99)$\varphi_{thermal}$		10×10 cm^2 to 40×40 cm^2 Φ_{total} = (2.08 ± 0.10)φ_{fast} + (24.44 ± 1.62)$\varphi_{thermal}$		10×10 cm^2 to 40×40 cm^2 Φ_{total} = (1.91 ± 0.09)φ_{fast} + (35.22 ± 3.84)$\varphi_{thermal}$	

$$\Phi_{total} = \left(SF + 1\right)\varphi_{fast} + \left(TF + 1\right)\varphi_{scatter}, \quad (13)$$

This equation is generally correct for all concrete types. Table 3 lists the scattering and thermal factors of the ordinary, limonite-steel, and magnetite-steel concretes at the isocenter (position 1) for all of the photon field sizes. According to Table 3, the total neutron fluence of the ordinary concrete at the isocenter has been obtained for field sizes from 15×15 cm^2 to 40×40 cm^2, as follows:

$$\Phi_{total} = \left(1.371 \pm 0.01\right)\varphi_{fast} + \left(53.28 \pm 1.99\right)\varphi_{thermal}. \quad (14)$$

The obtained total and direct neutron fluencies are (1.73 ± 0.12)×10^7 n cm^{-2}/Gy X-ray and (9.39 ± 0.85)×10^6 n cm^{-2}/GyX-ray, respectively, for the 5×5 cm^2 field size with and without the treatment room walls. According to Table 3, the SF + 1 coefficient is equal to 1.845; therefore, the value of 1.73×10^7 n cm^{-2}/GyX-ray is equal to 1.845×9.39×10^6 n cm^{-2}/GyX-ray. This analytical method should remain true for other field sizes and concretes; therefore, Eq. (13) can be replaced by Eq. (7) at the isocenter. Similarly, with the use of Eq. (13), the total neutron fluences of the magnetite-steel and limonite-steel concretes have been obtained for the 10×10 cm^2 to 40×40 cm^2 field sizes according to Eq. (15) and Eq. (16), respectively, as follows:

$$\Phi_{total} = \left(2.08 \pm 0.10\right)\varphi_{fast} + \left(24.44 \pm 1.62\right)\varphi_{thermal}, \quad (15)$$

$$\Phi_{total} = \left(1.91 \pm 0.09\right)\varphi_{fast} + \left(35.22 \pm 3.84\right)\varphi_{thermal}. \quad (16)$$

The high wt% of the iron nuclei and the low-threshold energy of the (γ,n) reaction may be the causes of the high scattering factor values of the magnetite-steel and limonite-steel concretes. But the scattering factors of the treatment rooms that are made of the magnetite-steel and limonite-steel concretes are 2.91 times and 2.45 times (with a 16% discrepancy) greater, respectively, than that of the ordinary concrete. Mesbahi et al. (2012) reported that the produced neutron fluence per n/m^2 per primary photon is 1.65×10^{-5} for ordinary concrete, but the value of 1.86×10^{-5} was derived for both the magnetite-steel and limonite-steel concretes. Although the neutron production factors are the same for the magnetite-steel and limonite-steel concretes in the above-referenced work, the scattering and thermal factors exhibit different values at the isocenter for the magnetite-steel and limonite-steel concretes in the present work.

For a treatment room that is made of ordinary concrete, the results

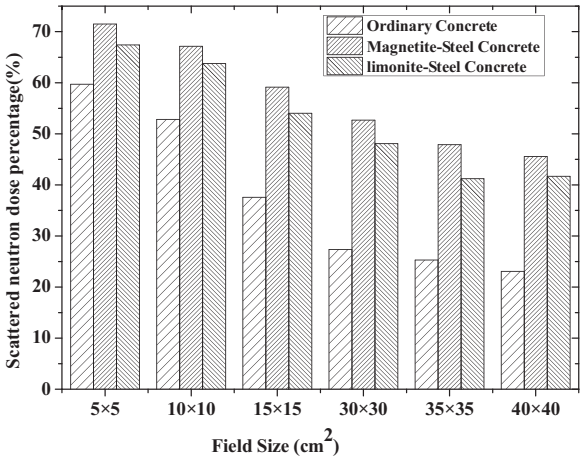

Fig. 10. The scattered neutron dose percentage for ordinary, magnetite-steel, and limonite-steel concretes.

show that the average energies of the direct and scattered neutrons at the isocenter are 0.7 MeV and 0.3 MeV, respectively, for all of the photon field sizes, which also conforms to the IAEA, 2006 report. According to the ICRU74, the conversion coefficient values of 375 and 233 have been selected for the direct and scattered neutrons, respectively. The average energy of the scattered neutrons in the treatment room with the magnetite-steel and limonite-steel concretes is 0.35 MeV, and the conversion coefficient is 258. Fig. 10 shows the scattered neutron dose contributions (%) to the patient at the isocenter for the ordinary, magnetite-steel, and limonite-steel concretes for different photon field sizes. According to Fig. 10, the scattered neutron dose contribution decreases with an increasing of the photon field size.

Table 4 shows the total scattered and direct neutron ambient dose equivalent (mSv/GyX-ray) at the isocenter for the ordinary, magnetite-steel, and limonite-steel concretes. The results here are in agreement with almost all of the previous works for a treatment room that is made of ordinary concrete, with the exception of the work undertaken by Ramírez et al., 2016. According to Table 4, and in relation to the simulations that have been undertaken in the published works (Ghassoun and Senhou, 2012), the simulation results of the present work represent a maximum discrepancy of 23%; however, a comparison with the other experiment data shows larger differences (approximately 40%). The maximum difference is regarding the work of Ramirez et al. (Ramírez et al., 2016), and this can be attributed to the following:

1) In the measurements performed by Ramirez et al., the TLD dosimeters were placed in a 10 cm spherical moderator, while in the present work, and based on the Monte Carlo evaluations, the optimal radius of the cylindrical moderator is 5 cm, and the detection of low-energy neutrons has not been compromised as a result.
2) The room dimensions in the work of Ramirez et al. are 8.95 m ×10 m (the wall-height information is missing), while the room dimensions in the present work are 7.5 m×7.5 m×3.8 m. The larger dimensions normally result in a lower neutron dose at the isocenter; moreover, the maze entrance in the work of Ramirez et al. is 1.8 m larger than that of the present work, and this causes a considerable fraction of the produced neutrons that escape from the treatment room and that are not detected at the isocenter.

Also, the room dimensions that were used in the work of Alem-Bezoubiri et al., 2014, are 6.45 m×7.37 m×4.18 m, and are approximately similar to the wall dimensions of the present work. But, the room dimensions that were used by Ghassoum et al., 2012, are 6 m×6 m×2.7 m, and are much smaller than the room that is considered in the present work. Small room dimensions normally result in larger neutron dose contributions at the isocenter. In addition, the MCNP tally and the LINAC head configuration that were used by Ghassoum et al. are different from what has been used in the calculations of the present paper.

According to Table 4, such neutron dose values are extremely harmful to the human body. Since the average photon dose to the patients is approximately 70 Gy for the course of a treatment (25–30 sessions), the total neutron doses to the patient are 259 ± 11.40 mSv, 463.05 ± 27.80 mSv, and 420.05 ± 24.78 mSv for the ordinary, magnetite-steel, and limonite-steel concretes, respectively, for a 10×10 cm^2 photon field. For a treatment room that is made of the magnetite-steel and limonite-steel concretes, the neutron doses to the patient are 1.79 and 1.62 times greater than that for the room made of ordinary concrete. It is well known that the biological damage increases with an increasing of the *linear energy transfer* (LET); therefore, the damage caused by heavier particles such as protons, alpha particles, heavy ions, and fission fragments are greater than the damage that is caused by electrons and positrons. The RBE values of the protons and other ions that normally recoil via neutron interactions are relatively greater than that of the photons in the patient body that signifies the neutron dose for radiotherapy.

4. Conclusion

This work presents the simulation results of the neutron dose from a medical LINAC to the patient with and without treatment room walls that are made of three different concrete types; for this purpose, the Monte Carlo N-particles MCNPX 2.6 code has been used. The results provide detailed information on the neutron contributions from the walls of the different concretes, and they also confirm that the neutron

Table 4
Total, scattered and direct neutron ambient dose equivalent (mSv/GyX-ray) at the isocenter for treatment rooms made of ordinary, magnetite-steel, and limonite-steel concretes.

Field size (cm^2)	Total dose (mSv/GyX-ray) _Ordinary concrete	Total dose (mSv/GyX-ray)_Other reported data_Ordinary Concrete				Total dose_ magnetite-steel (mSv/GyX-ray)	Total dose_limonite-steel (mSv/GyX-ray)
		MC	Difference (%)	Experimental	Difference (%)		
5×5	3.02 ± 0.15	–		–		5.32 ± 0.33	4.65 ± 0.26
10×10	3.70 ± 0.16	3.41 (Alem-Bezoubiri et al., 2014)	8	2.74 (Alem-Bezoubiri et al., 2014)	26	6.62 ± 0.40	6.00 ± 0.36
		3.13, (Howell et al., 2005)	15.4	2.21(Ramírez et al., 2016)	40		
		4.55, (Ghassoun and Senhou, 2012.)	23.0	–	–		
15×15	4.210.20	–	–	–	–	8.01 ± 0.46	7.12 ± 0.36
30×30	4.38 ± 0.17	3.78 (Alem-Bezoubiri et al., 2014)	13.70	3.43 (Alem-Bezoubiri et al., 2014)	21.70	8.38 ± 0.46	7.65 ± 0.39
35×35	4.19 ± 0.21	–	–	–	–	7.48 ± 0.45	6.64 ± 0.40
40×40	3.90 ± 0.21	–	–	–	–	6.86 ± 0.34	6.41 ± 0.37

dose is increased through the scattering that is off the walls of the treatment room. To reduce the thermal neutron dose it is necessary to use a thin layer of the thermal neutron absorber material around the patient body, with the exception of the desired photon pathway. Also, to reduce the neutron dose to the patient, a treatment room with low scattering and thermal factors is recommended.

Acknowledgment

These research were patricianly supported through the National Research Foundation of Korea (NRF) funded by the Ministry of Science, ICT & Future Planning (NRF-2015M2B2A4033123).

References

Al-Ghamdi, H., Al-Jarallah, M.I., Maalej, N., 2008. Photoneutron intensity variation with field size around radiotherapy linear accelerator 18-MeV X-ray beam. Radiat. Meas. 43, S495–S499.

Alem-Bezoubiri, A., Bezoubiri, F., Badreddine, A., Mazrou, H., Lounis-Mokrani, Z., 2014. Monte Carlo estimation of photoneutrons spectra and dose equivalent around an 18 MV medical linear accelerator. Radiat. Phys. Chem. 97, 381–392.

Bartesaghi, G., et al., 2007. A real time scintillating fiber dosimeter for gamma and neutron monitoring on radiotherapy accelerators. Nucl. Instrum. Methods Phys. Res. Sect. A: Accel. Spectrom. Detect. Assoc. Equip. 572 (1), 228–230.

Benites-Rengifo, J.L., Vega-Carrillo, H.R., Velazquez-Fernandez, J., 2014. Photoneutron spectrum measured with a Bonner sphere spectrometer in planetary method mode. Appl. Radiat. Isot. 83, 256–259.

Biltekin, F., Yeginer, M., Ozyigit, G., 2015. Investigating in-field and out-of-field neutron contamination in high-energy medical linear accelerators based on the treatment factors of field size, depth, beam modifiers, and beam type. Physica Med. 31 (5), 517–523.

Followill, D.S., Stovall, M.S., Kry, S.F., Ibbott, G.S., 2003. Neutron source strength measurements for Varian, Siemens, Elekta, and General Electric linear accelerators. J. Appl. Clin. Med. Phys. 4 (3), 189–194.

Gentilini, A., Rager, J.P., Steinmetz, K., Tacchi, M., Antonini, D., Arcipiani, B., Moioli, P., Pedretti, E., Scafé, R., 1980. Comparison of four calibration techniques of a silver activated Geiger counter for the determination of the neutron yield on the Frascati plasma focus experiment. Nucl. Instrum. Methods 172 (3), 541–552.

Ghassoun, J., Senhou, N., 2012. The evaluation of neutron and gamma ray dose equivalent distributions in patients and the effectiveness of shield materials for high energy photons radiotherapy facilities. Appl. Radiat. Isot. 70 (4), 620–624.

Howell, R.M., Ferenci, M.S., Hertel, N.E., Fullerton, G.D., 2005. Investigation of secondary neutron dose for 18 MV dynamic MLC IMRT delivery. Med. Phys. – N. Y.-Inst. Phys. 32 (3), 786–793.

Hsu, F.Y., Chang, Y.L., Liu, M.T., Huang, S.S., Yu, C.C., 2010. Dose estimation of the neutrons induced by the high energy medical linear accelerator using dual-TLD chips. Radiat. Meas. 45 (3), 739–741.

IAEA International Atomic Energy Agency, 2006. Radiation protection in the design of radiotherapy facilities. IAEA Safety Report Series No. 47.

IAEA International Atomic Energy Agency, 2000a. Calibration of radiation protection monitoring instruments,. Safety Reports Series No. 16.

IAEA International Atomic Energy Agency, 2000b. Handbook on photonuclear data for application cross section and spectra, TECDOC-Draft No.3.

ICRP, 1996. Conversion Coefficients for Use in Radiological Protection Against External Radiation vol. 74. Pergamon Press, Oxford, Publication, vol. 74.

ICRP International Commission on Radiological Protection, 2007. Recommendations of the International Commission on Radiological Protection. Publication 103 Valentin, pp. 1–34.

ISO8529; International Organization for Standardization, 1998. Reference neutron radiations – Part 3: (Calibration of area and personal dosimeters and determination of response as a function of energy and angle of incidence).

Janis, ⟨https://www.oecd-nea.org/janis/⟩.

Lin, J.P., Chu, T.C., Lin, S.Y., Liu, M.T., 2001. The measurement of photoneutrons in the vicinity of a Siemens Primus linear accelerator. Appl. Radiat. Isot. 55 (3), 315–321.

Liu, W.S., Changlai, S.P., Pan, L.K., Tseng, H.C., Chen, C.Y., 2011. Thermal neutron fluence in a treatment room with a Varian linear accelerator at a medical university hospital. Radiat. Phys. Chem. 80 (9), 917–922.

Mao, X.S., Kase, K.R., Liu, J.C., Nelson, W.R., Kleck, J.H., Johnsen, S., 1997. Neutron Sources in the varian clinac 21000/23000 medical accelerator calculated by the EGS4 code. Health Phys. 72 (4), 524–529.

McConn, R.J., Jr, Gesh, C.J., Pagh, R.T., Rucker, R.A., Williams III, R.G., 2011. Compendium of material composition data for radiation transport modeling. PNNL-15870 Rev. 1 (4).

Mesbahi, A., Azarpeyvand, A.A., Khosravi, H.R., 2012. Does concrete composition affect photoneutron production inside radiation therapy bunkers? Jpn. J. Radiol. 30 (2), 162–166.

Mesbahi, A., Keshtkar, A., Mohammadi, E., Mohammadzadeh, M., 2010. Effect of wedge filter and field size on photoneutron dose equivalent for an 18 MV photon beam of a medical linear accelerator. Appl. Radiat. Isot. 68 (1), 84–89.

Mohammadi, A., Afarideh, H., Davani, F.A., Arbabi, A., 2016. New aspect determination of photoneutron contamination in 18 MV medical linear accelerator. Radiat. Meas..

Naseri, A., Mesbahi, A., 2010. A review on photoneutrons characteristics in radiation therapy with high-energy photon beams. Rep. Pract. Oncol. Radiother. 15 (5), 138–144.

NCRP National Council on Radiation Protection and Measurements, 1993. Limitation of exposure to ionizing radiation, Report 116.

Pena, J., Franco, L., Gomez, F., Iglesias, A., Pardo, J., Pombar, M., 2005. Monte Carlo study of Siemens PRIMUS photoneutron production. Phys. Med. Biol. 50 (24), 5921.

Podgorsak, E.B., 2005. Radiation oncology physics. a handbook for teachers and students. International Atomic Energy Agency, Vienna, 657.

Ragabi moghaddam, S., Abbasi Davani, F., 2009. Design of activation counter cell for counting of fast neutron produced by plasma focus device. J. Nucl. Sci. Technol. 49, 1–5.

Ramírez, P.V.C., Díaz Góngora, J.A.I., Paredes Gutiérrez, L.C., Montalvo, T.R., Vega Carrillo, H.R., 2016. Neutron H*(10) estimation and measurements around 18 MV LINAC. Appl. Radiat. Isot.. http://dx.doi.org/10.1016/j.apradiso.2016.05.006.

Shweikani, R., Anjak, O., 2015. Estimation of photoneutron intensities around radiotherapy linear accelerator 23-MV photon beam. Appl. Radiat. Isot. 99, 168–171.

Takam, R., 2010. Evaluation of Normal Tissue Complication Probability and Risk of Second Primary Cancer in Prostate Radiotherapy (Doctoral dissertation). School of Chemistry and Physics, The University of Adelaide.

Thalhofer, J.L., Roque, H.S., Rebello, W.F., Correa, S.A., Silva, A.X., Souza, E.M., Batita, D.V.S., Sandrini, E.S., 2014. Effect of external shielding for neutrons during radiotherapy for prostate cancer, considering the 2300 CD linear accelerator and voxel phantom. Radiat. Phys. Chem. 95, 267–270.

Vega-Carrillo, H.R., Manzanares-Acuña, E., Iñiguez, M.P., Gallego, E., Lorente, A., 2007. Study of room-return neutrons. Radiat. Meas. 42 (3), 413–419.

Xu, X.G., Bednarz, B., Paganetti, H., 2008. A review of dosimetry studies on external-beam radiation treatment with respect to second cancer induction. Phys. Med. Biol. 53 (13), R193.